Chemical Engineering Journal 94 (2003) 241–254

Chemical Engineering Journal

www.elsevier.com/locate/cej

Residence time distribution of droplets within discs and doughnuts pulsed extraction columns via Lagrangian experiments and simulations

N. Bardin-Monnier*, P. Guiraud, C. Gourdon

Laboratoire de Génie Chimique, UMR 5503 CNRS-INP/ENSIACET-UPS, 18 Chemin de la Loge, F3 1078 Toulouse Cedex 04, France

Accepted 29 January 2003

Abstract

This paper is devoted to the study of the transport of single droplets in discs and doughnuts extraction pulsed columns. Video experiments are carried out on a pilot plant of industrial size ($D = 300$ mm) in order to extract the values of the plug flow with axial dispersion transport model parameters (i.e. mean residence time and axial dispersion coefficient). The same kind of results are established thanks to Lagrangian simulations carried out with the industrial computational fluid dynamics (CFD) code ESTET (EDF, SIMULOG). A detailed study of the influence of the simulation conditions (expressions of the forces, turbulent dispersion and rebound modelling) is led in order to set the limits of such an approach. The agreement between experiments and simulations is around 20%. This study leads to the conclusion that the quality of the results seems to depend strongly on the prediction of the continuous phase flow turbulence.

Keywords: Extraction column; Two-phase flow; Lagrangian tracking; CFD; Axial dispersion; Pulsed flow

1. Introduction

Solvent extraction is one of the most widely used unit operations involved in process industry. This mass transfer operation consists in separating one or several substances (solute) present in a solid or a liquid phase by contacting it with another liquid phase in which these substances are preferentially transferred. This unit operation is often processed in column type contactors within which the two immiscible phases flow countercurrently under the effect of gravity, one being mechanically dispersed into the other. By way of example, the contactor considered here is the discs and doughnuts pulsed column (Fig. 1), mainly used in the nuclear wastes treatment. It is composed of successive stages delimited by discs and doughnuts, alternately arranged along a cylindrical pipe. The countercurrent flow maintains high concentration gradients between the phases allowing efficient mass transfer all along the contactor.

This efficiency is clearly related to the hydrodynamics of both phases. Like in the case of other packed columns, the major design problem of the such contactors lies in the choice of the geometrical parameters of the packing and of the pulsation conditions, responsible for the hydrodynamic behaviour. A mechanically imposed pulsation makes the flow unsteady and turbulent. This pulsation of the flow in this baffled complex geometry produces shearings and turbulence which generate breakage of the droplets and, as a consequence, sufficient interfacial area required for mass transfer. Furthermore, recirculations created by the packing ensure a long enough contact time between the phases. Nevertheless, axial mixing takes place within the column and reduces the efficiency of the process by decreasing solute concentration gradients and as a consequence the mass transfer rate. For this reason, this axial mixing, affecting both phases, has to be reduced at its lowest level [1], and has to be taken into account in the design of industrial columns. Neglecting these phenomena inevitably leads to an overevaluation of the process efficiency.

The usual process engineering approach to represent the hydrodynamic behaviour of such contactors is based on simplified transport models for both phases, the most common one appearing to be the plug flow with axial dispersion model [2]. As far as the contactor considered in this paper is concerned, many experimental studies have been led about the axial dispersion of the continuous phase [3–5]. These experimental methods consist in measuring the residence time distribution (RTD) of an electrolytic (or radioactive) tracer through several compartments of the column. To characterise the hydrodynamic behaviour of the dispersed phase,

* Corresponding author. Present address: LSGC-ENSIC, 1 rue Grandville, BP 451-54001 Nancy Cedex, France. Tel.: +33-3-8317-5346; fax: +33-3-8317-5086.
E-mail address: nmonnier@ensic.inpl-nancy.fr (N. Bardin-Monnier).

1385-8947/03/$ – see front matter
doi:10.1016/S1385-8947(03)00055-X

Nomenclature

a	coefficient of the Langevin's model
A	pulsation amplitude (m)
b	coefficient of the Langevin's model
C	constant
C_β	ratio of the Lagrangian integral timescale to the Eulerian integral timescale
C_d	drag coefficient
C_m	added mass coefficient
d_p	droplet diameter (m)
dt	time step (s)
D	diameter (m)
$\mathcal{D}_{id}$	axial dispersion coefficient of the dispersed phase (m^2/s)
e	random Gaussian velocity (m/s)
Eo	Eötvos number ($=g\Delta\rho d_p^2/\gamma$)
f	pulsation frequency (Hz)
g	gravity acceleration (m/s^2)
G	gravity centre
H	disc–doughnut spacing (m)
k	turbulent kinetic energy (m^2/s^2)
L	length of the column (m)
M^i	ith order moment of the spatial or temporal distributions, s^i or m^i
Mo	Morton number ($=(g(\Delta\rho)\rho_f\mu_f^4)/(\rho_f^2\gamma^3)$)
n	entire number
Pe	Peclet number ($=v_d L/\mathcal{D}_{id}$)
r_c	restitution coefficient
r_t	residence time in a compartment (s)
Re_p	particle Reynolds number ($=(d_p\|\|u(x_p(t),t)-v_p(t)\|\|)/(v_f)$)
t	time (s)
t_c	mean residence time in a compartment (s)
t_m	mean residence time on a length L of the column (s)
T	pulsation period (s)
T^*	packing free area
T_E	Eulerian integral timescale of the fluid (s)
T_L	Lagrangian integral timescale of the fluid (s)
T_L^*	Lagrangian integral timescale of the fluid seen by the droplets (s)
$u(x_p(t), t)$	instantaneous velocity of the continuous phase at the drop position (m/s)
$u'(t)$	turbulent fluid velocity seen by the droplet (m/s)
U_{max}	permanent component of the bulk velocity (m/s)
$u_p\ (t)$	periodic component of the bulk velocity (m/s)
v_d	mean velocity of a monodispersed population (m/s)
$v_p(t)$	instantaneous droplet velocity (m/s)
$v_{pn}(t)$	instantaneous normal velocity before the rebound (m/s)
$v_{pt}(t)$	instantaneous tangential velocity before the rebound (m/s)
$v_{p'n}(t)$	instantaneous normal velocity after the rebound (m/s)
$v_{p't}(t)$	instantaneous tangential velocity after the rebound (m/s)
v_t	free fall velocity of the droplets (m/s)
We	Weber number ($=\rho_f v_t^2 d_p/\gamma$)
$x_p(t)$	instantaneous droplet position

Greek letters

γ	interfacial tension (N/m)
ε	dissipation rate of the turbulent kinetic energy (m^2/s^3)
ν_f	kinematic viscosity of the fluid (m^2/s)
ρ	density (kg/m^3)
σ	S.D. of the RTD (s)

Subscripts

d	dispersed phase
di	disc
do	doughnut
f	fluid
in	inlet of the central compartment
out	outlet of the central compartment
ref	reference value

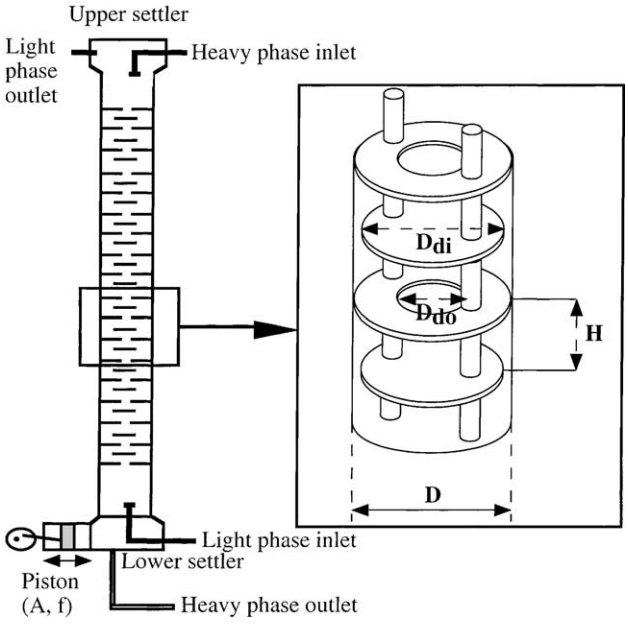

Fig. 1. The discs and doughnuts extraction column.

the same kind of technique has been used [5], but also "single drop experiments" in which the residence time distributions are obtained by measuring the individual residence time of a set number of drops. Such kind of studies have been led on Kühni columns [6,7] but also on discs and doughnuts pulsed columns [8]. Both kinds of experiments have to be repeated for many geometrical and operating conditions in order to correlate the behaviour to these conditions. Nevertheless, this experimental approach presents two major disadvantages. On one hand, it is very long, tedious and sometimes impossible to be performed in the case of very large columns, and, on the other hand, these kinds of experiments made on pilot plants do not allow to solve the problem of scale-up.

The aim of this paper is to study the ability of Lagrangian simulations to replace these "single drop experiments". The computational fluid dynamics (CFD) offers an interesting alternative in the description of the hydrodynamic working of contactors, such as extraction columns, whatever the size, the internal design, and the operating conditions. For single-phase flows in the same column type running under a wide range of operating and geometric conditions, Aoun Nabli et al. [9,10] have established hydrodynamic behaviours and correlation for axial mixing coefficient via CFD numerical experimentations.

Lagrangian simulations of single drop trajectories can be considered as the numerical counterpart of the single drop experiments. However, modelling of the forces acting on the drops, turbulent dispersion, droplet–wall interaction, and simulation strategy still remain key problems of this kind of approach. This paper is focused on two main objectives: the first one is to establish a simulation strategy corresponding to the "single drop experiments", and the second one is to evaluate the accuracy of these numerical experiments in relation to industrial design and to point out the main improvements that have to be introduced in the different modelling levels. For given geometric and operating conditions, simulations results are compared with experimental ones in term of residence time distribution and plug flow with axial dispersion transport model parameters (i.e. mean residence time in a compartment and axial dispersion coefficient).

In the first part of the paper, the experimental set-up and the metrology are described. Secondly, details are given about modelling and numerical treatments. In this part, the strategy and tools of simulation are explained. The last part is dedicated to the aforementioned comparisons for different simulation conditions.

2. Experiments

2.1. The discs and doughnuts column

The column used to perform the experiments (Fig. 1) is composed of a 2 m high vertical 0.288 m in diameter cylindrical Perspex pipe. It contains a packing constituted by 3×10^{-3} m thick stainless steel discs and doughnuts alternately arranged conferring a 23.5% open-free area to the device. The packing elements are maintained by 4.5×10^{-2} m length and 1×10^{-3} m diameter stainless steel braces ($H = 0.0048$ m), giving to the ensemble a spatial periodicity. A 0.288 m diameter pipe including three openings of 1.25×10^{-1} m and separated by 120° forms the foot of the column. This pipe is coupled to the pulsation system thanks to a cylindrical jacket. The pulsation system is of mechanical type with counter pressure. It is composed of a piston driven by a crank-arm system with variable lever-arm length, dragged by a direct current system that allows variable amplitude and frequency until 4×10^{-2} m and 3 Hz, respectively. The chosen operating conditions correspond to a 1.65×10^{2} m amplitude A and to a frequency f of 1 Hz. The flow generated is purely oscillating following (1):

$$u_p(t) = \pi A f \cos(2\pi f t) \quad (1)$$

2.2. Measurement system

The residence time distribution of the droplets is established by following the trajectories of 2.5×10^{-3} m in diameter calibrated drops thanks to a video system on two stages of the column (Fig. 2). Toluene drops coloured by red Cerol-Soudan IV are injected in a water continuous phase thanks to a pushing syringe pump HARVARD apparatus type 44 and a stainless steel capillary penetrating into the column. At the end of the capillary, a cylindrical Perspex pipe has been placed to avoid a too early detaching of the droplets due to the pulsation of the continuous flow. The syringe has a diameter of 3.24×10^{-3} m (syringe KOELHN of 500×10^{-9} m^3). Droplets are injected five compartments under the visualisation section, itself located in the middle part of the column and surrounded by a square Perspex box filled with water in order to avoid optical distortions. Two 500 W halogeneous spotlights enlighten this part and a white cover has been placed behind the column to obtain an uniform

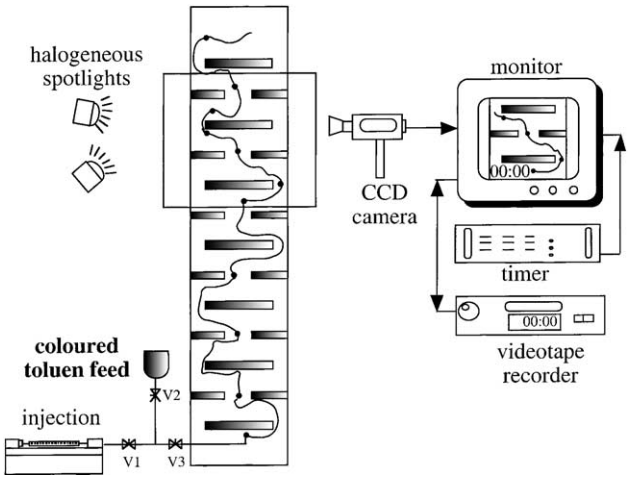

Fig. 2. The experimental set-up.

light repartition. Drop trajectories crossing three stages of the column are filmed thanks to a FAIRCHILD CCD video camera. Trajectories are recorded by a JVC S-VHS HR5900 MS video tape recorder linked to an electronic video-timer that allows the inscription of the time on the image at a precision of 10^{-2} s.

2.3. Physico-chemical properties of the phases

Experiments are performed at ambient temperature with a tap-water continuous phase and toluene-red Cerol-Soudan IV solution droplets. As the density of the drops is less than the one of the continuous phase, the drops naturally rise in the column. The density of the dispersed phase is measured using a hydrometer or density bottle. The results show that its value is not modified by the presence of the dye (866.2–866.7 kg/m^3 instead of 867 kg/m^3 for pure toluene). On the contrary, the interfacial tension between the two phases (measured by a hanging drop technique and by the Wilhelmy method) shows appreciable decrease with an increase of the Cerol-Soudan IV concentration from 35.4×10^{-3} N/m for pure toluene to 3.4×10^{-3} N/m in the case of 10^{-3} kg/kg toluene dye concentration. Thus, in order to ensure a sufficient coloration of the drops and an interfacial tension not too low to avoid the breakage of the droplets, a dye concentration of 5×10^{-5} kg for 1 kg of toluene is used. The corresponding interfacial tension value is 30.5×10^{-3} N/m.

2.4. Unfolding of the experiments

One hundred drops are injected one by one at sufficiently high time steps in order not to have two drops in the camera-field at the same time. After each experiment, recorded films are viewed at a low speed and the residence time of each drop in two successive stages is noted. These data are treated to obtain the residence time distribution on these elements of the column.

3. Lagrangian simulations

3.1. Hypothesis and modelling

The numerical experiments deal with a two-phase unsteady (pulsed) turbulent flow via an Euler–Lagrange method. The pulsed continuous phase flow is simulated as a function of the time thanks to the resolution of Reynolds averaged mass and momentum conservation equations. Turbulence is taken into account thanks to a k–ε model associated to logarithmic wall laws for this phase. This model is based on two main hypotheses, which are the isotropy of turbulence and a local spectral equilibrium. As mentioned by Aoun Nabli et al. [9], the first condition is not generally fulfilled in complex flows, such as the one under consideration in this study, but the good results of a great number of simulations show that only satisfaction at a small scale of this isotropy hypothesis seems to be necessary. The second hypothesis has been verified by spectral analysis of laser Doppler velocimetry measurements of flow velocities in the same contactor [4], revealing a $-5/3$ slope for the inertial range of the spectrum (5–100 Hz) in the case of an oscillation frequency around 1 Hz.

As far as the dispersed phase is concerned, the Lagrangian approach adopted in this work consists in simulating the behaviour of a cloud of droplets, following individually a great number of them. Generally, the movements of the two phases are strongly coupled, drops are agitated and carried by the surrounding fluid meanwhile their presence also influence and modify the continuous phase flow. This influence is directly linked to the volume fraction of the drops. At very low volume fractions, the influence of the drops on the carrier phase can be neglected (one way coupling hypothesis). That is obviously the case for "single drop numerical experiments". The drops considered in this study are also supposed to be spherical and rigid due to the relatively high value of the interfacial tension and to the drop size.

Each drop trajectory is obtained solving the fundamental law of dynamics taking into account the (a) buoyancy, (b) pressure gradient, (c) drag, (d) added mass forces induced by the unsteady Eulerian-simulated continuous flow as follows:

$$\begin{aligned}\frac{\pi d_p^3}{6}\rho_d\frac{dv_p(t)}{dt} &= \underbrace{\frac{\pi d_p^3}{6}(\rho_d-\rho_f)g}_{a} + \underbrace{\rho_f\frac{\pi d_p^3}{6}\frac{Du(x_p(t),t)}{Dt}}_{b} \\ &+ \underbrace{\frac{1}{2}\frac{\pi d_p^2}{4}\rho_f C_d||u(x_p(t),t)-v_p(t)||(u(x_p(t),t)-v_p(t))}_{c} \\ &+ \underbrace{\frac{\pi d_p^3}{6}C_m\rho_f\left(\frac{Du(x_p(t),t)}{Dt}-\frac{dv_p(t)}{dt}\right)}_{d} \end{aligned} \quad (2)$$

Many expressions have been proposed for the drag coefficient C_d [11]: the physico-chemical properties of the phases, the kind of flow and the inclusion type are parameters that have to be taken into account in the choice of the C_d correlation. Schiller and Nauman's (3.a) and Newton's (3.b) ones have been chosen in this study because they seem to be the most reliable in the case of solid particles [11] and undeformable drops [12].

$$C_d = \frac{24}{Re_p}(1+0.15Re_p^{0.687}), \quad Re_p \le 1000 \quad (3.a)$$

$$C_d = 0.44, \quad Re_p > 1000 \quad (3.b)$$

Nevertheless, for liquid–liquid systems, other kinds of correlations taking into account the drop deformation have been established thanks to the study of the drop movement in a stagnant unbounded liquid. In this case, the free fall velocity

of the drops is linked to the drag coefficient through the classical relation (4):

$$v_t(d_p) = \left(\frac{4}{3} g \frac{\Delta\rho}{\rho_f} d_p\right)^{0.5} C_d^{-0.5} \quad (4)$$

C_d expressions are derived from correlations available for the free fall velocity [13]. For the system of phases considered here, Stokes' (5.a) and Vignes' (5.b) laws are as follows:

$$C_d = \frac{24}{Re_p}, \quad Re_p < 1 \quad (5.a)$$

$$C_d = 5.6 Re_p \frac{1}{We} Mo^{1/3} \left(1 - \frac{Eo}{6}\right), \quad 1 < Re_p \leq 1000 \quad (5.b)$$

In order to verify if Schiller and Nauman's and Newton's laws can be used, a comparison has been made with the C_d values issued from Vignes' law in the range of observed particle Reynolds numbers in the flow under consideration. Fig. 3 illustrates the evolution of the particle Reynolds number for a drop crossing the simulation domain. The operating conditions are the following ones: $A = 1.65 \times 10^{-2}$ m, $f = 1$ Hz, $d_p = 2.5 \times 10^{-3}$ m. Re_p ranges from 20 to 800. Fig. 4 shows that Schiller and Nauman's law does not differ from Vignes' one in this particle Reynolds numbers range. Moreover, Schiller and Nauman's law ensures continuity with Newton's one for particle Reynolds numbers higher than 1000, avoiding numerical jumps in the Lagrangian treatment.

The value of the added mass coefficient C_m is taken as 0.5 [14]. Taking into account this force in the trajectories equation may be a subject of controversy in so far as the 0.5 C_m value has only been established in the case of solid spheres and spherical bubbles [15]. Furthermore, the turbulent dispersion model used in this work generates continuous but non-differentiable velocities seen by the drops, what induces approximations in the force balance. As a consequence, tests have been carried out in order to quantify the influence of the added mass force.

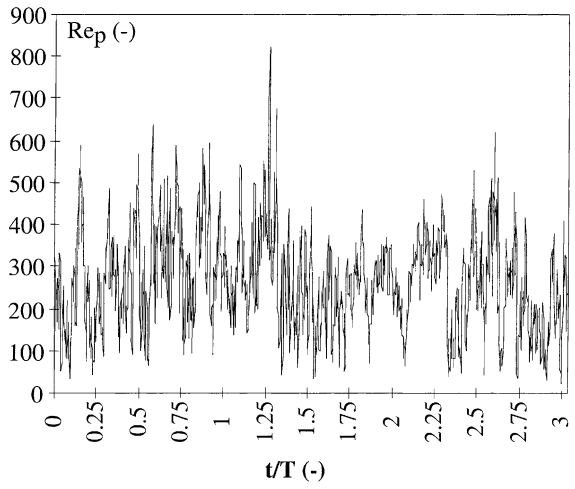

Fig. 3. Evolution of the Reynolds number of the particle as a function of the dimensionless time.

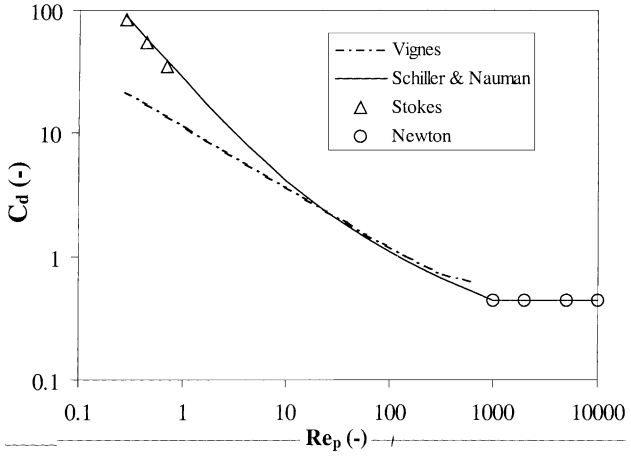

Fig. 4. Evolution of the drag coefficient as a function of the Reynolds number of the particle.

The effect of the continuous phase flow turbulence on the drops (i.e. the turbulent dispersion) is modelled thanks to a simplified Langevin's equation [16]. This kind of model is based on the hypothesis that both longitudinal and transversal Eulerian spatial integral scales are equal and that the probability distribution function of the fluctuating velocities follows a Gaussian law. The turbulent velocity seen by a drop at a given time step, and from the local turbulence level like the next equations express:

$$u'(t = (n+1)\,dt) = a\,u'(t = (n)\,dt) + be \quad (6)$$

with

$$a = \exp\left(\frac{-dt}{T_L^*}\right), \qquad b = \sqrt{1 - a^2},$$

e = random Gaussian variable,

$$T_L^* = \frac{T_L}{1 + C_\beta(||u(x_p(t), t - v_p(t))||)/(\sqrt{2k/3})}, \quad C_\beta = \frac{T_L}{T_E} \quad (7)$$

Resorting to this kind of model still sets some questions principally induced by the turbulent scale value prediction, directly linked to the local values of k and ε. In the next part of this paper, answers are proposed thanks to sensitivity tests.

3.2. Calculation domain

The experimental works of Oh [4] and Angelov et al. [17] on this contactor show that the mean flow is two-dimensional and axisymmetrical, but that the turbulence is three-dimensional. The packing shows a spatial periodicity. Each compartment represents a spatial pattern, constituted

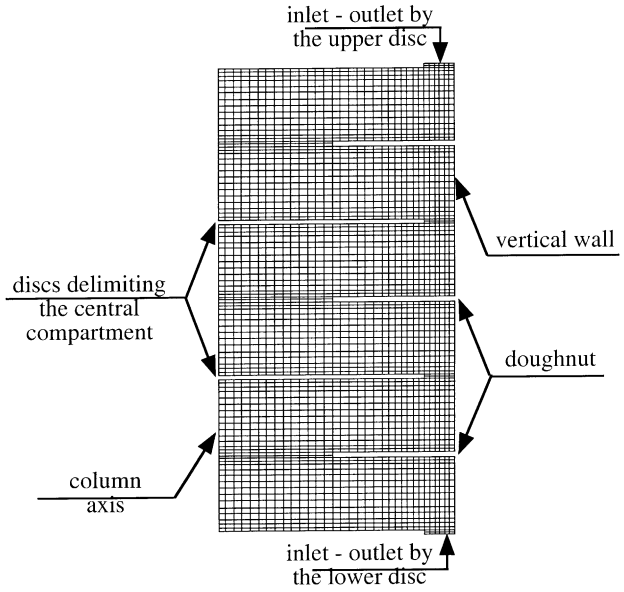

Fig. 5. Simulation domain.

of two stages, each delimited by successive disc–doughnut or doughnut–disc. Considering these characteristics, continuous flow calculations are performed in two dimensions between the axis and the wall of the column using cylindrical co-ordinates (r, z) on three compartments, which is a sufficient number to establish the flow [18]. The structured and irregular mesh used to discretize the domain (Fig. 5) is composed of:

- thirty-three radial lines, 6 of which are in the free area of the disc and 14 in the free-area of the doughnut;
- fourteen axial lines separate two baffles and two represent their thickness.

As far as the Lagrangian step is concerned, the particle transport is three-dimensionally calculated. The mean velocity of the surrounding fluid has no tangential component; nevertheless, the instantaneous velocities taking part in the force balance have a non-zero tangential component, what induces particle displacement in this direction. The simulated trajectories take into account these displacements, but the simulation plane follows the tangential location of the drops while their tangential velocity is kept.

Boundary conditions apply only to the continuous phase and are similar to the ones used by Aoun Nabli et al. [9].

3.3. Calculation strategy

The calculation strategy is composed of three steps. In a first time, the permanent flow corresponding to the maximal amplitude of pulsation is simulated until the establishment of the flow. Secondly, the inlet flow rate is pulsed until reaching a locally periodic flow. Once this continuous phase flow established, the study of the dispersed phase can start. Drops are injected in the downward compartment on 16 points of the mesh around the doughnut. The initial velocity is the one of the fluid and this injection starts just when the flow starts its upward acceleration phase. Once the drops enter the last stage they are re-positioned two compartments downward with the same radial position and the same velocity. This method is used in order to simulate the working of a high column with a great number of compartments, what would consume too much time and memory. In order to fit the experimental work, where droplets enter or exit naturally the measurement compartment because they have been injected far from it, the height of the column is replaced in the simulation work by several crossings of the simulation domain. This technique can be used because of the axial spatial periodicity of the column.

Calculations are performed until the establishment of the dispersed phase flow, what means that the entry or exit of the droplets in the compartment is not influenced by the injection conditions. This establishment is considered to be reached when the spatial periodicity of the radial entrance distributions in two successive compartments and the temporal periodicity of the entrance distributions along a period are completed. For each crossing of the 2400 drops in the central compartment (the evaluation of the influence of the drop number has shown that 2400 drops is sufficient), the aforementioned distributions are plotted and the three first moments M^i (Eq. (8)) of each distribution are calculated and compared thanks to an "error" function defined as follows:

$$\text{error} = \frac{|M^i_{\text{in}} - M^i_{\text{out}}|}{|M^i_{\text{in}}|} \tag{8}$$

where M^i_{in} is the ith order moment of the radial position distribution at the entry of the compartment (respectively of the entrance time distribution) and M^i_{out} is the same moment of the ith order at the exit of the compartment.

Fig. 6a and b show the evolution of these errors as a function of the number of crossings. A global decrease is noticeable and both errors do not exceed 4% after the third crossing in the case under consideration.

Fig. 7a and b show the resulting radial and temporal distributions, respectively. In the first graph, preferential entrance or exit radial positions at the limit of the disc (60% in number) can be noticed. In the second graph, which deals with the temporal analysis, namely 80% of the drops enter or exit the compartment when the continuous flow is ascending ($-0.25T$ to $0.75T$) and a large part of them ($\sim$54%) during its upward acceleration phase ($-0.25T$ to T). These results are in good agreement with those experimentally obtained by Laulan [8] and with the observations on the experimental plant.

When the establishment of the drop flow is confirmed, the residence time distributions are stored on each stage. These distributions are then used to calculate the parameters of the plug flow with axial dispersion transport model.

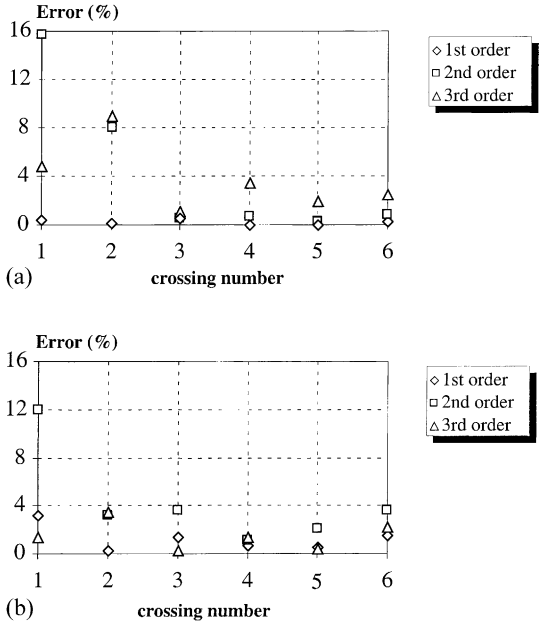

Fig. 6. Comparison between the three first moments of the: (a) radial inlet and outlet distributions; (b) temporal inlet and outlet distributions.

3.4. Evaluation of the plug flow with axial dispersion transport model parameters

Given the residence time distributions in two successive stages, the RTD in a greater number of elements of the column are rebuilt thanks to a convolution algorithm [8].

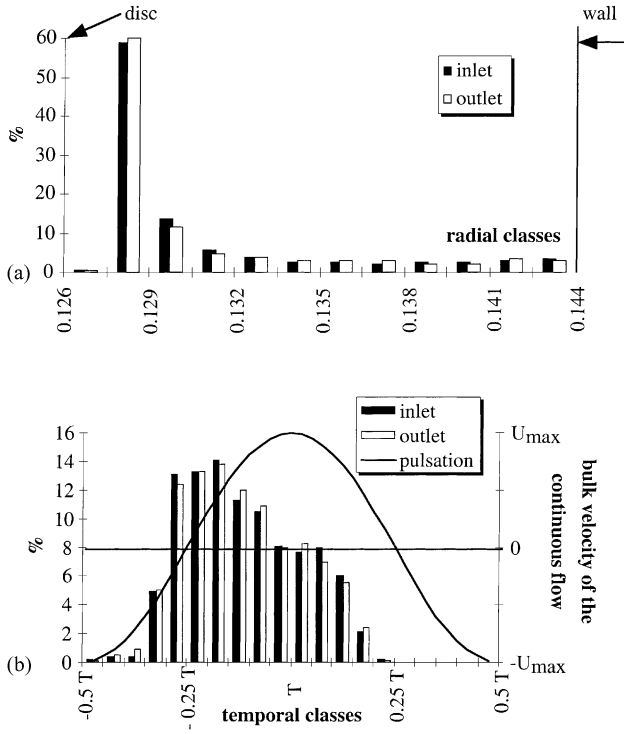

Fig. 7. (a) Radial inlet and outlet distributions. (b) Temporal inlet and outlet distributions.

For each resulting distribution on k stages, the mean value and the variance of the distribution are calculated. Thanks to these data, the Peclet number is evaluated, considering that the k stages form an open area for dispersion both at the entrance and exit by the relation (9) [19]:

$$\frac{\sigma^2}{t_m^2} = \frac{2}{Pe} + \frac{8}{Pe^2} \tag{9}$$

The axial dispersion coefficient is then calculated following (10), where L is the length of the k stages, and v_d the mean velocity of the dispersed phase:

$$Pe = \frac{v_d L}{\mathcal{D}_{id}} \tag{10}$$

This convolution procedure is carried out until reaching a constant value of the axial dispersion coefficient and of the mean velocity of the dispersed phase, i.e. until the considered column length is sufficient to represent the behaviour of the dispersed phase by a plug flow with axial dispersion one-dimensional transport model. In fact, the RTD obtained on each stage show two peaks (Figs. 9, 10 and 12), what can not be represented by a plug flow with axial dispersion. Nevertheless, this model is suitable for a more important length of the column, where the RTD curves exhibit only one peak. In this study, the stabilisation occurs after 32 stages.

The next part shows the results obtained by Lagrangian simulations in terms of droplet trajectories and residence time distributions. A thorough study is then led on the influence of the simulation conditions via comparisons of the RTD and transport model parameters with experimental values.

4. Simulation results and comparison with experimental data

4.1. Droplet trajectories

Fig. 8a and b both show drop trajectories obtained by the way of simulation. The different marks represent each quarter of period as mentioned on the bottom of Fig. 8a. These trajectories have been chosen because they are representative of all the behaviours encountered in the simulations. The droplets enter or exit each stage preferentially near the edge of the packing elements (disc or doughnut) just when the flowing velocity is ascending. This fact can be related to the observations led for the whole number of drops in Fig. 7a and b. For example, in Fig. 8a, it can be noticed that the drop penetrates in each stage during these lapses of time. This preferential tendency is especially noticeable during the ascending acceleration phase of the flowing velocity between $0.75T$ and T and principally around $0.75T$. Actually, between $0.5T$ and $0.75T$, the flow in the column is negative; the droplets are stopped at the edge of the packing elements (Fig. 8b near the disc at the bottom of the central compartment). When the flow becomes zero around $0.75T$,

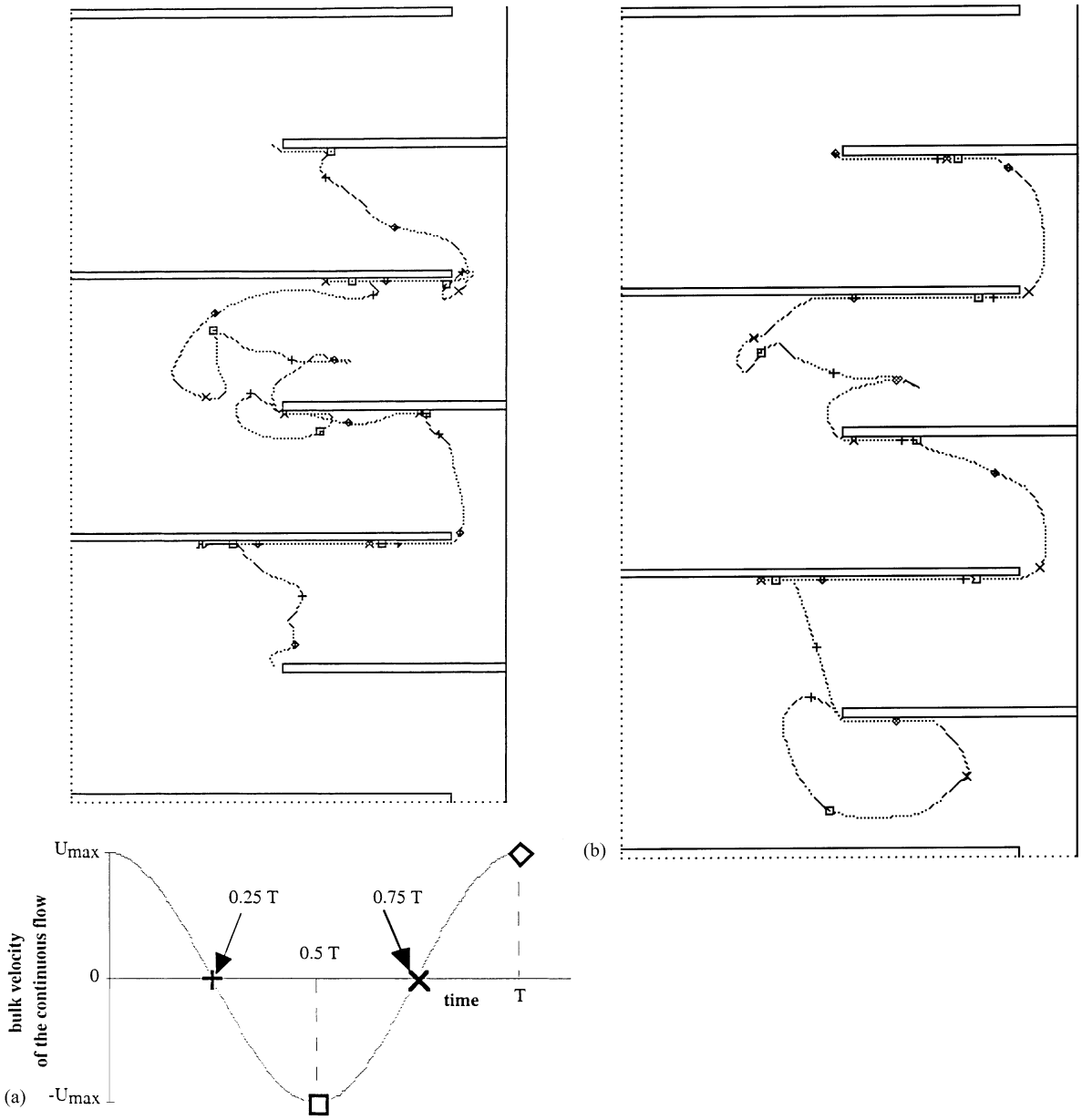

Fig. 8. (a and b) Examples of a particle trajectory.

the velocities are positive at the edge of the discs and the doughnuts: the droplets, whose axial displacement has been stopped by the packing, are carried by the continuous flow and exit the stage. When they enter a stage during the first quarter of the period, the droplets are generally recaptured by the downward flow during the second quarter of the period (Fig. 8b near the doughnut of the downward compartment). The droplets never come close to the axis of the column because this area corresponds to large dead zone of the continuous flow. The behaviour of the continuous phase is not presented here but can be found in [9]. The last feature that can be observed is a strong wall–droplet interaction. In fact, the residence time of the droplets is partially linked to the time they spend under the packing elements (this interaction time may represent 10–50% of the residence time in a stage). This interaction is more important with the discs than with the doughnuts. This phenomenon may be explained by the fact that the recirculations generated at the doughnut level are bigger than the ones generated at the disc level. So, when the droplets pass round the recirculations, they arrive farther from the disc edge than from the doughnut one.

4.2. Residence time distribution in each stage

The next result presented concerns the residence time distributions in each stage for a drop diameter of 2.5×10^{-3} m. The experimental and numerical distributions appear in Fig. 9 (note that the stage 1 corresponds to a stage

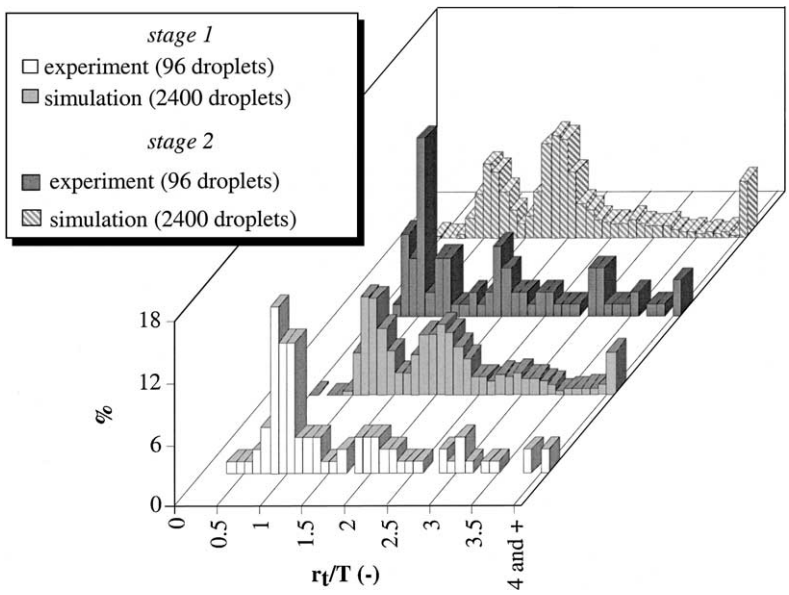

Fig. 9. Experimental and numerical residence time distributions on two stages of the column.

of type disc–doughnut and the stage 2 to a stage of type doughnut–disc). In this figure, the radial axis represents the residence time expressed as a function of the period and the axial one the percentage of droplets whose residence time is equal to each class of time. The analysis of this figure leads the following remarks. First, for each type of stage, the numerical RTD are multi-modal with peaks appearing around residence times equal to entire number of periods: the same tendency can be found for the experimental ones. This multi-modal shape can be explained by the fact that the droplets enter or exit the central compartment when the flowing velocity is ascendant, like aforementioned. As far as the numerical RTD are concerned, it can be noticed that a gap is present between the RTD in stage 1 and stage 2. For the stage 1, the major peak is situated around T, while for the stage 2, this one is displaced around $2T$. This gap may be due to the more important interaction of the droplets with the disc than with the doughnut as shown in the previous section. This gap does not appear in the experimental results: for each stage, the major peaks are situated around T. Nevertheless, for the experimental RTD the peak at $2T$ is more important for the stage 2 than for the stage 1. Secondly, the numerical RTD reveals that the droplet proportion whose residence time is more than four periods is more important in the stage 2 than in the stage 1 (6 for 4% in the stage 1). This propensity to spend more time in the stage 2, which is also found again experimentally (3.5 for 2%), can be explained by the same reasons as the previous ones. Both these behaviours induce a residence time more important in the stage 2 than in the stage 1 (the mean values for the whole population are 1.9 5 and 2.16 5 numerically). The experimental results for these operating conditions show the same tendency (1.54 s for the stage 1 and 1.92 s for the stage 2). Finally, for each stage, a gap between the experimental and numerical RTD can be noticed: for example, in the case of the stage 2, the first RTD starts at $0.9T$ while for the second one, the droplets exit the stage as soon as the second quarter of period. Furthermore, the drop proportion staying in one stage more than four periods is more important for the simulation results.

To sum-up, the comparison between experimental and numerical RTD has shown that they both have the same multi-modal shape and that a gap is present between them. But, despite this gap, the results in terms of plug flow with axial dispersion model parameters show an agreement around 20% for all the parameters (mean residence time in a compartment and axial dispersion coefficient), as it is underlined by Table 1.

As a conclusion of this paragraph, it is obvious that Lagrangian simulations of droplet trajectories inside contactors such as discs and doughnuts extraction columns are source of primordial information about the hydrodynamic behaviour of the droplets. Even if a gap is present, the comparison in terms of RTD between experimental and numerical results is quite satisfying with a design objective, for which no other tools are able to give this kind of information at an industrial scale. But it is clear that modelling improvements still have to be performed for more accurate results. In order to lighten the main modelling points on which these improvements have to be made, sensitivity tests

Table 1
Comparison between the experimental and numerical mean residence time and axial dispersion coefficient

	Experiment	Simulation
Mean residence time (s)	3.35	3.92
Axial dispersion coefficient ($\times 10^{-4}$ m^2/s)	2.3	1.8

at different modelling levels are presented in the following section.

4.3. Influence of the simulation conditions

This paragraph intends to show the results obtained with different simulation conditions. This study is led as following: for each parameter of simulation the discussion is made about the RTD: comparisons are made between the experimental RTD, the "standard" RTD and the ones where the simulation conditions have been changed. Based on these RTD, a comparison is also made on the mean residence time and on the axial dispersion coefficient.

4.3.1. Influence of the added mass force

Taking into account the added mass force in the solving of the trajectory equation requires the knowledge of the instantaneous velocity field "seen" by the droplet. The turbulent component of the velocity "seen" is calculated thanks to a Langevin's model, which generates continuous but non-differentiable velocities. As a consequence, using this kind of model induces a simplification of the added mass force expression, where the mean component of the velocity is only taken into account. Moreover, the 0.5 value for the added mass coefficient has been established only in the cases of solid spheres and spherical bubbles. Simulations have then been led without taking into account this force in order to evaluate its impact on the droplet transport.

Fig. 10 represents the RTD obtained via experiments and via simulations (standard simulation with the added mass force and modified one without it). The multi-modal shape of the RTD is unchanged when the added mass force is not taken into account. Nevertheless, peaks around residence times around one or two periods are clearly more pronounced. The RTD tends to be narrower around these two peaks. It can also be noticed that the drop proportion that stay in the stage during one pulsation period is more important than in the standard simulation, what seems to be more in agreement with the experimental results. Moreover, the drop percentage whose residence time is more than three periods is far less important (4%) when the added mass force is not considered in the simulations compared to the experimental RTD and the one issued from the standard simulation (12 and 14%, respectively). Results in terms of mean residence time and axial dispersion coefficient are also given in Fig. 10. Without the added mass force, the mean residence time is lessened, the gap with regards to the experimental value is reduced. The higher value of the residence time when taking into account the added mass force may be due to the fact that this inertia force tends to impede any relative "droplet carrier fluid" acceleration; in fact, it tends to reduce the droplet slip velocity. As far as the axial dispersion coefficient is concerned, like the RTD narrow shape allowed to foresee, $\mathcal{D}_{id}$ is quite lower than in the standard simulation. This added mass force impact on the axial dispersion can be explained by coming back to the physical sense of this force. When the droplet has a relative acceleration with regards to the carrier flow, this force tends to slow the drop, while the impact is opposite when the carrier flow acceleration is superior to the droplet one. These acceleration situations are induced by the pulsation and associated gradients in the continuous phase flow due to the pulsation and by the fact that the droplets cross high velocity gradients. On the contrary, turbulence does not take part here because only the mean component of the fluid velocity seen by the droplet is taken into account in the added mass force expression (Eq. (2)).

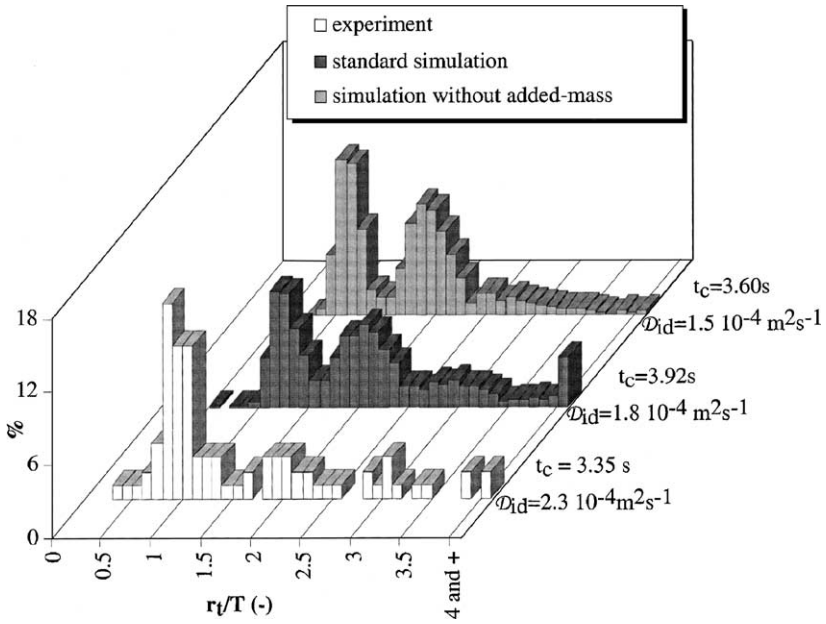

Fig. 10. Influence of the added mass force on the RTD and plug flow with axial dispersion model parameters.

As a consequence, the omission of this force in the trajectory equation leads to the decrease of the droplet velocity variations. At the whole droplet population level, this fact induces a decrease of the axial dispersion.

As a conclusion about the influence of the added mass force in the droplet trajectory equation, it can be noticed that taking this force into account leads to an increase of the droplet velocity distribution and allows to reduce the gap between experiments and simulation. Nevertheless, the opposite conclusion could be made from residence time point of view. Explanations have been put to the fore but the experimental uncertainties remain key problems for a suitable comparison.

4.3.2. Rebound modelling

As it has been observed on the droplet trajectories (Fig. 8a and b), the droplet–wall interactions play an important role on the behaviour of the dispersed phase. These interactions are managed by a rebound type treatment, acting on the normal velocity of the droplet arriving on the wall, via a restitution coefficient r_c. If for gas solid systems the value of this restitution coefficient is certainly close to 1, in the case of droplets carried by a liquid r_c can not be fixed on the basis of actual knowledge. As a consequence, sensitivity of the RTD to changes of r_c values is reported here. Three r_c values are tested: a case corresponding to an elastic rebound ($r_c = 1$), a case without rebound, drops only slipping along the walls after contact ($r_c = 0$), and an intermediate situation ($r_c = 0.5$). In Fig. 11, the three simulated situations are presented: after the first contact (Fig. 11a), the drop is relocated at a distance from the wall equal to its radius, its tangential velocity v_{pt} is not modified, but its normal velocity v_{pn} changes to $-r_c\ v_{pn}$ (Fig. 11b–d for $r_c = 1$, 0.5 and 0, respectively). The resulting RTD are presented in Fig. 12. First, it can be noticed that the restitution coefficient decrease does not modify the multi-modal shape of the RTD. Nevertheless, for restitution coefficients equal to 0.5 or 0, the major peak is located around residence times equal to two pulsation periods, while for the standard numerical ($r_c = 1$), and experimental RTD this peak is located around one pulsation period. Moreover, the droplet proportion that stay in the stage during more than four pulsation periods increases with the decrease of the restitution coefficient (it reaches 9% for a zero restitution coefficient). As a conclusion, the decrease of the restitution coefficient leads to RTD which do not tend to better fit the experimental results. As far as the transport model parameters are concerned, Fig. 12 underlines that the decrease of the restitution coefficient inevitably leads to an increase of the mean residence time, what is not surprising: the lower the restitution coefficient is, the more the droplets are sticked on the walls, and as a consequence are not recaptured by the continuous flow and are globally slowed down. On the contrary, the axial dispersion coefficient slightly varies with the restitution coefficient, due to the combining of the slowing down by drop–wall interactions and of the dispersion effects acting on droplets being recaptured by the flow.

4.3.3. Turbulent dispersion

The behaviour of droplets carried by the continuous liquid phase is clearly managed by the instantaneous velocity field they see, which is turbulent in the case under consideration here. However, due to the impossibility to solve directly this instantaneous velocity field, only the mean components of the fluid velocity are calculated, the turbulence being accounted via its kinetic energy k and its dissipation rate ε. The trajectory (Eq. (2)) and the formulation of the forces involved are derived from the instantaneous balance of the forces acting on the drop. In order to solve the trajectory equation, it is then necessary to rebuild an instantaneous velocity. This aim is completed thanks to a turbulent dispersion model (see Section 3.1). In fact, it has been shown [20]

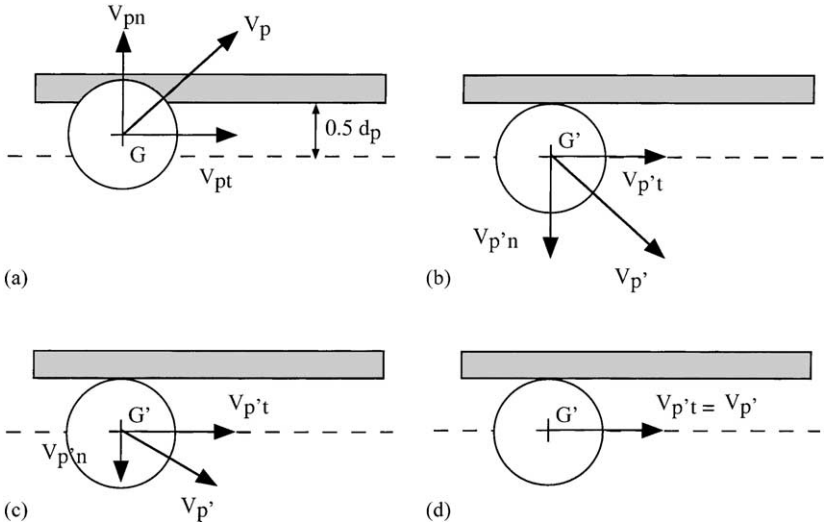

Fig. 11. Rebound modelling.

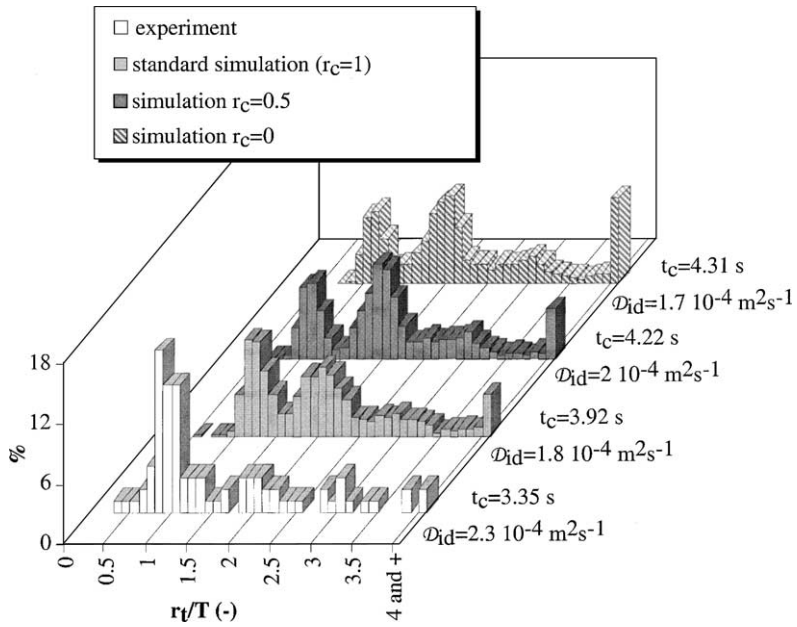

Fig. 12. Influence of the restitution coefficient on the RTD and plug flow with axial dispersion model parameters.

that the omission of the turbulent component of the fluid velocity seen by the droplet leads to deterministic trajectories, far from the real behaviour of the drops in the column. The resulting instantaneous velocity obviously depends on the parameters of the turbulent dispersion model used and on the local values of k and ε seen by the droplets.

The main sensitive turbulent dispersion model parameter is the Lagrangian integral timescale T_L. This timescale represents the time a fluid particle spends in a turbulent structure and its value conditions the amplitude of the turbulent fluid velocity component seen by the droplet. T_L is related to the local values of k and ε thanks to the following relation [21]:

$$T_L = C\frac{k}{\varepsilon} \tag{11}$$

The value of the constant C is still a subject of controversy in the literature [16]. In the standard simulation cases, C is fixed to 0.2 and has been modified from 0.1 to 0.5.

As far as the prediction of the turbulent variables k and ε is concerned, it is well known that their prediction in complex flows are still far from being accurate, even if the resulting mean flow is well predicted. In order to drastically test their influence on the turbulent dispersion, they have been arbitrarily multiplied or divided by 2.

The results are presented in terms of the transport model parameters. In Fig. 13a and b, which deal with the mean residence time, it can be noticed that both these simulation parameters have a great influence. When C or k and ε increase, the turbulent component of the fluid velocity seen by the drop increases, what induces strong droplets trajectory perturbations and, as a consequence, an increase of the mean residence time. By shifting C from 0.1 to 0.5, the mean residence time varies by about 13%, and a change concerning the local k and ε values from 0.5 to 2 their initial values induces a 20% variation. The effects on the axial dispersion coefficient are stronger (Fig. 14a and b), the variations being

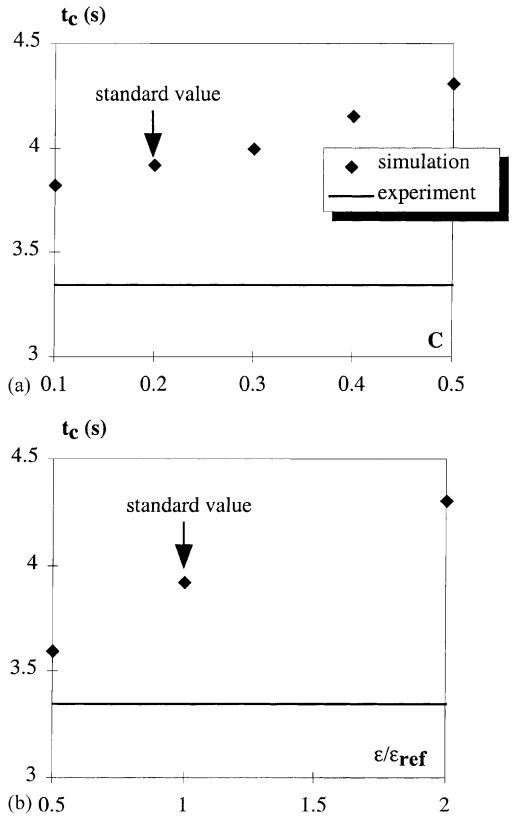

Fig. 13. Influence of the turbulent dispersion model on the mean residence time: (a) C constant of the model; (b) value of the turbulent dissipation.

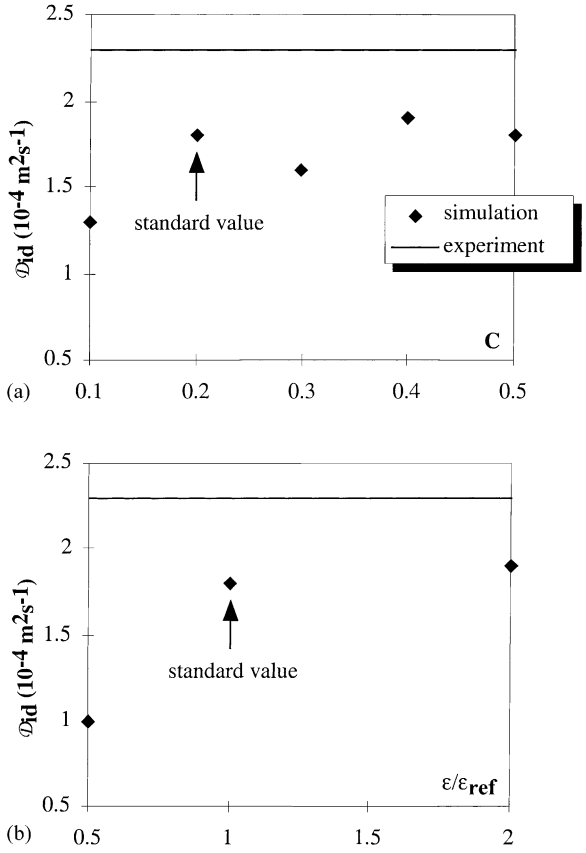

Fig. 14. Influence of the turbulent dispersion model on the axial dispersion coefficient: (a) C constant of the model; (b) value of the turbulent dissipation.

about 46% as a function of C and about 86% as a function of k and ε. Referring to the experimental mean residence time, these results should lead to the conclusion that the constant C and the turbulent variables k and ε are over-evaluated, but this conclusion does not agree with the results concerning the axial dispersion coefficient. In fact, for the lower values of the parameters governing the turbulent velocity seen by the droplets, the axial dispersion strongly decreases, like Fig. 14a and b underline.

5. Discussion

As a conclusion of this paragraph concerning the influence of the simulation conditions, it is obvious that the knowledge of the expressions of the forces acting on the droplets remains the basis of an accurate representation of drops behaviour by Lagrangian simulations. If the expression of the added mass force and its treatment in a turbulent case certainly have to be improved, other forces, neglected here due to the lack of knowledge in such complex flows, like Basset force and mainly lift forces, should have to be accounted. However, the use of quite precise expressions for each force is only efficient if the behaviour of the continuous phase is perfectly predicted. It seems that a k–ε model of turbulence associated with wall laws cannot give this required level of description, mainly in the areas close to the walls. In fact, a more accurate modelling of the drop–wall interactions cannot be performed without a better description of the turbulent bursts occurring near these walls, responsible for the coming back of the droplets in the bulk. The rebound modelling should be revisited after this better description of the continuous flow. In our point of view, it should be interesting to try another description of the continuous velocity field, thanks to a Large Eddy Simulation type approach for instance. The same kind of Lagrangian study as the one presented here could then be led in order to quantify if the trajectory equation and the rebound modelling used are efficient.

6. Conclusion

This work intends to quantify the ability of Lagrangian simulations to represent the hydrodynamic behaviour of single droplets in a disc and doughnut pulsed column. Measurements of residence time have been performed on a pilot plant thanks to a video technique in order to set a data bank for validation. A numerical Lagrangian tracking has been led on the basis of a simulated continuous phase flow, turbulence being accounted thanks to a k–ε model. The trajectory equation is solved taking into account the drag, added mass, pressure gradient and buoyancy forces. The turbulent dispersion of the droplets is linked to the carrier flow turbulence thanks to a modified Langevin's model. These simulations have been led with the industrial CFD code ESTET (EDF, SIMULOG).

Both experimental and numerical results show that the residence time on one stage exhibits a multi-modal distribution, with main peaks around entire numbers of pulsation periods, due to the fact that droplets enter in and exit of the stages when the continuous flow is in the first part of its ascending phase. The behaviour of the drops is partially managed by drop–wall interactions which are more sensitive in the doughnuts to discs type stages, leading to more important residence time in this kind of stages.

The comparisons between experimental and numerical results in terms of plug flow with axial dispersion model parameters show an agreement around 20% for all the parameters (mean residence time in a compartment and axial dispersion coefficient). Even if a gap remains, this comparison is quite satisfying as a design objective, for which no other tools are able to give this kind of information at an industrial scale like the one treated in this work.

As far as the simulation conditions are concerned, the sensitivity tests about the expressions of added mass force, rebound modelling and turbulent dispersion modelling which have been made seem to question the turbulent dispersion calculation. This calculation depends, on one hand, on the simulation of the continuous flow turbulence, and on the

other hand, on the model itself. At first sight, it may be thought that it should be necessary to come back to the calculation of the turbulence of the continuous flow before any change in the Lagrangian equation or in the dispersion model. Secondly, necessary improvements have to be performed on the modelling of the droplet–wall interaction, both when the droplets arrive near the walls and when they collide with them. Here again, a more accurate calculation of the continuous flow is a key point. It should be interesting to test a new way of simulation of the continuous flow, which might consists in a Rij transport model or Large Eddy Simulation approach. On the basis of this simulation, the same type of Lagrangian tracking should be led. The last interesting perspective of this work deals with the simulation of industrial applications. In fact, in most of them, the hold up of the dispersed phase is greater than 15%, and as a consequence affects the continuous phase flow. The simulation of the flows in these cases can be performed using the "two-way coupling" approach that consists in taking into account the influence of the dispersed phase on the continuous phase flow. Nevertheless, in our point of view, the most promising approach lies in the "two fluid model". This simulation technique induces that both phases are considered as fluids which interact with each other. Equations concerning mean velocity, kinetic energy and turbulence characterising the whole dispersed phase are solved. Transfer terms between the phases are taken into account by introducing source terms in the continuity and masse balance equations.

Acknowledgements

This work was performed with the financial and technical supports of Electricité de France (EDF). The authors would like to thank Mr. Jean-Pierre Minier for his help with the Lagrangian modelling.

References

[1] N.N. Li, E.N. Ziegler, Effect of axial mixing on mass transfer in extraction columns, Ind. Eng. Chem. 59 (3) (1967) 30–36.
[2] T. Miyauchi, T. Vermeulen, Diffusion and back-flow models for two phases axial dispersion, Ind. Eng. Chem. Fundam. 2 (1963) 304–310.
[3] H.-H. Park, Analyse du fonctionnement d'une colonne d'extraction à disques et couronnes, Ph.D. Thesis, Institut National Polytechnique de Toulouse, France, 1980.
[4] W.Z. Oh, Analyse du fonctionnement hydrodynarnique d'une colonne pulsée à disques et couronnes, Ph.D. Thesis, Institut National Polytechnique de Toulouse, France, 1983.
[5] M.F. Buratti, Etude des phénomènes de mélange axial dans les colonnes pulsées équipées de garnissage disques-couronnes, Ph.D. Thesis, Institut National Polytechnique de Lorraine, France, 1988.
[6] M. Cabassud, Analyse de la rupture des gouttes—contribution à la simulation d'une colonne Kühni, Ph.D. Thesis, Institut National Polytechnique de Toulouse, 1987.
[7] I. Seikova, C. Gourdon, G. Casamatta, Single drop transport in a Kühni extraction column, Chem. Eng. Sci. 47 (1992) 4141–4154.
[8] A. Laulan, Hydrodynamique et rupture de gouttes dans une colonne pulsée à disques et couronnes, Ph.D. Thesis, Institut National Polytechnique de Toulouse, France, 1980.
[9] M.S. Aoun Nabli, P. Guiraud, C. Gourdon, Numerical experimentation: a tool to calculate the axial dispersion coefficient in discs and doughnuts pulsed solvent columns, Chem. Eng. Sci. 52 (1997) 2353–2368.
[10] M.S. Aoun Nabli, P. Guiraud, C. Gourdon, CFD contribution to a design procedure for discs and doughnuts extraction columns, IchemE 76 (1998) 951–960.
[11] R. Clift, J.R. Grace, M.E. Weber, M.E. Bubbles, Drops and Particles, Academic Press, New York, 1978.
[12] M. Ischii, N. Züber, Drag coefficient and relative velocity in bubbly, droplet or particulate flows, AIChE J. 5 (1979) 843–855.
[13] C. Gourdon, G. Casamatta, G. Muratet, Population balance based modelling of solvent extraction columns, in: Liquid–Liquid Extraction Equipment, Wiley, New York, 1994, pp. 137–226.
[14] T.R. Auton, J.C.R. Hunt, M. Prud'homme, The force exerted on a body in inviscid unsteady non-uniform rotational flow, J. Fluid. Mech. 197 (1988) 241–257.
[15] J. Magnaudet, M. Rivero, J. Fabre, Accelerated flows past a rigid sphere or a spherical bubble. Part 1. Steady straining flow, J. Fluid. Mech. 284 (1995) 97–135.
[16] J.P. Minier, J. Pozorski, Analysis of existing Lagrangian models and new propositions for particle dispersion in homogeneous stationary turbulence, Rapport EDF, KE-44/92.29, 1992.
[17] O. Angelov, E. Journé, A. Liné, C. Gourdon, Simulation of the flow patterns in a disc and doughnut column, Chem. Eng. J. 45 (1990) 87–97.
[18] S. Le Garrec, Modelisation et simulation numerique de l'écoulement et de la dispersion dun contaminant dans une colonne pulsée, Ph.D. Thesis, Conservatoire National des Arts et Métiers, Paris, 1993.
[19] O. Levenspiel, Chemical Reaction Engineering, Wiley, New York, 1972.
[20] N. Bardin-Monnier, Simulations et expériences Lagrangiennes d'écoulements diphasiques en colonne pulsée à garnissage disques-couronnes, Ph.D. Thesis, Institut National Polytechnique de Toulouse, France, 1998.
[21] S.B. Pope, Lagrangian PDF methods for turbulent flows, Annu. Rev. Fluid Mech. 26 (1994) 23–63.